Fast algorithm based on triplet Markov fields for unsupervised multi-class segmentation of SAR images

WU Yan[1]*, WANG Xin[1], XIAO Ping[2], GAN Lu[1], LIU ChunYan[1] & LI Ming[3]

[1]*School of Electronics Engineering, Xidian University, Xi'an 710071, China;*
[2]*Shaanxi Bureau of Surveying & Mapping, Xi'an 710054, China;*
[3]*National Key Laboratory of Radar Signal Processing, Xidian University, Xi'an 710071, China*

Abstract Non-Gaussian triplet Markov fields (TMF) model is suitable for dealing with multi-class segmentation of non-stationary and non-Gaussian synthetic aperture radar (SAR) images. Considering the complexity of the model and algorithm, as well as the requirement of real-time, and robust and efficient processing of SAR images, a fast algorithm based on TMF for unsupervised multi-class segmentation of SAR images is proposed in this paper. For the speckle noise in SAR images, numerical characteristic, threshold selection and QuadTree decomposition criterion are researched firstly. With the new method, a SAR image can quickly be mapped into an edge-based pixon-representation, which results in a coarse decomposition in smooth regions, and a fine decomposition in edges. Then by combining TMF model with the pixon-representation of SAR image, a new potential energy function of TMF based on pixon-representation is derived. Finally, the segmentation is finished by Bayesian maximum posterior mode (MPM). The effectiveness of the fast TMF algorithm is demonstrated by applying it to simulated data and real SAR images.

Keywords pixon-representation of SAR image, QuadTree decomposition, new potential energy function, triplet Markov fields, multi-class segmentation

1 Introduction

Synthetic aperture radar (SAR) image segmentation is an important part of target recognition and interpretation of SAR images. It can provide the overall structure of the image information, reveal the nature of SAR images, establish the basis of automatic target recognition (ATR) and promote applications of SAR. In recent years it has gradually become a research hotspot both at home and abroad. Because of speckle produced by coherent electromagnetic irradiation during imaging, traditional optical image segmentation algorithms cannot suppress noise, which will lead to misclassifications. So they are not suitable for SAR image segmentation.

Recently, the development of statistical theory has opened up an effective way to analyze and model images. However, hidden Markov models (HMMs) are too simple to deal with a large number of complex

---

*Corresponding author (email: ywu@mail.xidian.edu.cn)

images (non-stationary images, texture images, strong noisy images). They can satisfactorily deal with stationary images [1, 2] but are powerless to treat non-stationary SAR images. So far their own statistical model has been constantly expanded and improved, making it possible to deal with non-stationary images and related non-Gaussian noise more efficiently. One of the effective extensions of HMMs is the triplet Markov fields (TMF) [3–11], which well describes the statistical characteristic of SAR images. In the case of two random fields X and Y of Markov random fields (MRF) model, TMF have been proposed in which a third random field U is introduced, and the triplet $T = (X, Y, U)$ is assumed to be Markovianity [8]. One possible meaning for $U = (U_s)_{s \in S}$ is to use $U = u$ to define different homogeneities of (X, Y). This means that the Markov field distribution $p(x, y/u)$ is a non-stationary field and the m possible values of U_s describe m different Markov non-stationarities (m-MNS) of (X, Y). Consequently this model is very suitable for dealing with the non-stationary SAR images in which the pixel values of image have random mutations caused by multiplicative speckle noise.

When using TMF algorithm to deal with large SAR images, we have to calculate the potential energy function with the four neighbors or eight neighbors of each pixel, and then calculate the distribution of the triplet (X, Y, U). The large amount of computation reduces the efficiency of the algorithm. In this paper, we try to introduce the concept of pixon into the TMF. This concept was first proposed by Pina and Puetter [12], whose essence is that the spatial scale at each site of an image varies according to the information embedded in the image, implying that the picture information can be dealt with by using cells of variable sizes corresponding to the local spatial information. In this way the optimal scale description of images is realized. Yang et al. [13] introduced a new pixon definition scheme for segmentation, whose shape and size can vary simultaneously, and they used the anisotropic diffusion equation to extract the pixons in their definition scheme. Then they combined the pixon concept and MRF model to reduced computation cost. On this basis, Lin et al. [14] proposed a classical QuadTree combination algorithm to extract the pixon-representation of natural images.

In this paper, for SAR images with speckle noise, we combine the pixon concept and TMF model to improve the computation efficiency of TMF segmentation algorithm. First we propose a new QuadTree decomposition for the speckle in SAR images: we introduce the region noise level σ_i, and then establish some new criterions of decomposition discriminant and threshold selection. Thus we obtain a coarse decomposition in smooth regions and a fine decomposition in edges. Finally we obtain an edge-based pixon-representation of SAR image. By combining TMF model with the pixon-representation of SAR image, the new potential energy function of TMF based on pixon-representation and the new segmentation formula of Bayesian maximum posterior mode (MPM) [15] are derived. The fast TMF algorithm is used to segment simulated data and real SAR images. Experimental results and analysis demonstrate that the fast TMF algorithm can effectively suppress the influence of speckle in SAR images, and greatly reduce the complexity of the algorithm and the running time without affecting the performance of segmentation. The fast TMF algorithm realizes the real-time, and robust and efficient processing of SAR image segmentation.

2   Non-Gaussian triplet Markov fields (TMF) model

Let S be the set of pixels. The MRF model contains two random fields defined on S, $X = (X_s)_{s \subset S}$ and $Y = (Y_s)_{s \subset S}$. The random X_s and Y_s take their values in $\Omega = \{\omega_1, \ldots, \omega_k\}$ and R, respectively. The problem of the statistical segmentation is how to recover the unobservable X from the observed Y [1, 2]. The possible nonstationarity of the distribution $p(x, y)$ of the (X, Y) is managed by introducing a third random field $U = (U_s)_{s \subset S}$. Thus the m possible values of U_s are interpreted as m different possible stationarities of (X, Y). Let $Z = (X, Y)$ be a pairwise random field. Then Z has an m-Markov nonstationarity [8]. If there is a random field $U = (U_s)_{s \subset S}$ each U_s taking its value in a finite set $\Lambda = \{\lambda_1, \ldots, \lambda_k\}$, then the triplet $T = (X, U, Y)$ is a stationary Markov field. When the set $U = (U_s)_{s \subset S}$ is simple enough, the TMF makes Bayesian processing possible and makes it possible to estimate $X = (X_s)_{s \subset S}$ from $Y = (Y_s)_{s \subset S}$.

Let us denote by C the set of cliques. Directly consider the Markovianity of the couple (X, U), and suppose that $\Lambda = (a, b)$ is limited to two states of (X, Y) which represent a set of stationarities. The

energy of the TMF model is then written as

$$W(x,u) = \sum_{(s,t)\in\mathbb{C}_H} \alpha_H^1(1 - 2\delta(x_s, x_t)) - (\alpha_{aH}^2\delta^*(u_s, u_t, a) + \alpha_{bH}^2\delta^*(u_s, u_t, b))(1 - \delta(x_s, x_t))$$
$$+ \sum_{(s,t)\in\mathbb{C}_V} \alpha_V^1(1 - 2\delta(x_s, x_t)) - (\alpha_{aV}^2\delta^*(u_s, u_t, a) + \alpha_{bV}^2\delta^*(u_s, u_t, b))(1 - \delta(x_s, x_t)), \quad (1)$$

where C_H (or C_V) is the set of couples of pixels' horizontal (or vertical) neighbors, and

$$\delta^*(u_s, u_t, a) = \begin{cases} 1, & u_s = u_t = a, \\ 0, & u_s \neq u_t, \end{cases} \qquad \delta^*(u_s, u_t, b) = \begin{cases} 1, & u_s = u_t = b, \\ 0, & u_s \neq u_t. \end{cases} \quad (2)$$

Then suppose that the random fields $Y = (Y_s)_{s\subset S}$ are not independent of $X = (X_s)_{s\subset S}$, and the distributions $p(y_s|x_s)$ would not be necessarily Gaussian. Assume that there are k classes $\Omega = \{\omega_1, \ldots, \omega_k\}$ and we want to have k densities $h_1, \ldots, h_k$, possibly of different forms, for the k distributions $p(y_s|x_s = \omega_1), \ldots, p(y_s|x_s = \omega_k)$. Let G be the cumulative distribution function of Gaussian zero-mean variable with variance one and let $H_1, \ldots, H_k$ be the cumulative distribution functions corresponding to $h_1, \ldots, h_k$. Let us consider the following TMF (X, U, Y):

1. Take a Markov field (X, U) with energy W.

2. Consider $Y' = (Y_s')_{s\in S}$ Gaussian Markov random field, where each Y_s' zero-mean, with variance one is

$$p(y') = \gamma \exp\left[-\frac{1}{2}\left(\sum_{s\in S}(y_s')^2 + \sum_{(s,t)} -\beta_1 y_s' y_t'\right)\right] = \gamma \exp[-W'(y')]. \quad (3)$$

3. For each $s \in S$, put $Y_{s\in S} = H_{X_{s\in S}}^{-1} \circ G(Y_{s\in S}')$. Finally, the distribution of the (X, U, Y) is defined as

$$p(x, u, y) = \gamma \exp\left[-W(x, u) - W'(\varphi(x, y)) + \sum_{s\in S} \log\left|\frac{\partial(G^{-1} \circ H_{x_s}(y_s))}{\partial y_s}\right|\right], \quad (4)$$

where $\varphi(x, y) = y' = (Y_S')_{s\in S}$. The TMF model given by eq. (4) can estimate $p(x_s|y)$ in two steps: 1) estimate $p(x_s, u_s|y)$ by the Gibbs sampler [16, 17]; and 2) calculate $p(x_s|y) = \sum_{u_s\in\Lambda} p(x_s, u_s|y)$. Therefore, the Bayesian MPM can be used in TMF given by eq. (4).

3 Fast algorithm based on TMF for unsupervised multi-class segmentation of SAR images

In this section we propose a fast segmentation algorithm. When using TMF algorithm to deal with large SAR images, the large amount of computation reduces the efficiency of the algorithm. Here we try to introduce the concept of pixon into the TMF to reduce computational cost. In subsection 3.1, the criterion of the new QuadTree decomposition based on speckle of SAR images is established to obtain a pixon-representation of SAR images. In subsection 3.2, a new potential energy function based on pixon-representation is derived. Finally the method of parameter estimation is given in subsection 3.3.

3.1 New QuadTree decomposition and pixon-representation of SAR image

First we give the definition of pixon as follows: S is the set of all image pixels, and $P_i = \{s_i\}_{i=1}^{n_i}$, where n_i is the number of pixels in P_i. If and only if all pixels in P_i are connected, P_i is called the ith pixon of the image [14]. Pixon-representation of image is defined as follows. A set of pixons, $P = \{P_i\}_{i=1}^N$, is a pixon-representation if and only if: 1) $P_i \neq \emptyset$; 2) $P_i \bigcap P_j = \emptyset$ if $i \neq j$; 3) $\bigcup_{i=1}^N P_i = S$.

The definition above shows that the pixon-representation segments the image into a set of disjoint regions, as shown in Figure 1(a). A set of edges can be acquired from these regions, $\boldsymbol{n} = \{\boldsymbol{n}_{i,j}|P_i, P_j \in P$ and P_i, P_j are adjacent$\}$, where the direction of $\boldsymbol{n}_{i,j}$ is from ith pixon P_i to jth pixon p_j, and $|\boldsymbol{n}_{i,j}|$ is equal to the length of the boundary between the two adjacent pixons P_i and P_j. The pixons combined with their edges construct a graph, which represents the observed image S, as shown in Figure 1(b).
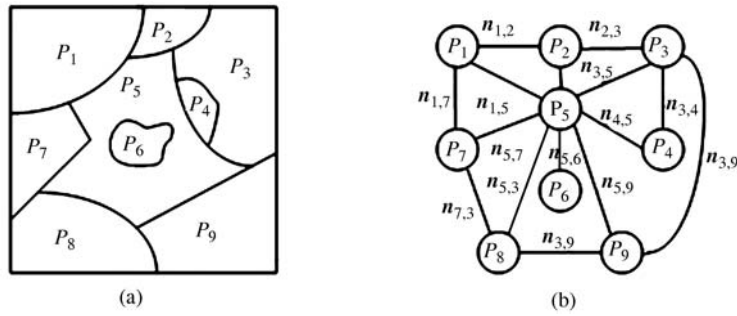
Figure 1   An example of pixon-representation. (a) The pixon map; (b) the corresponding graph.

In this paper we use the QuadTree decomposition to get the pixon-representation of images. Let $\max_S$ and $\min_S$ respectively be the maximum and minimum pixel value in the region to be decomposed. T_c is the threshold. The process of classical QuadTree decomposition is as follows. If $f_c = (\max_S - \min_S) < T_c$ is false for the initial region, the region will be decomposed into four smaller regions. Then taking the four regions as the initial region, repeat steps above until $f_c = (\max_S - \min_S) < T_c$ is true for all regions.

However, due to the speckle in SAR images, when using classical QuadTree decomposition to deal with SAR images, the following phenomenons may occur. For too small a threshold T_c, we will obtain redundant pixons and for too large a threshold T_c, we will lose a lot of details. In this paper, we introduce the numerical characteristic noise level σ_i to solve this problem. σ_i is defined as the noise standard variance of the ith region, which denotes the stationary level of this region. If σ_i is too large, there will be edges or multi-class in this region.

Combined with the noise level, a new QuadTree decomposition method with double-discriminants is used to decompose SAR images. The steps are as follows.

Step 1: Find out the maximum and minimum pixel values of the initial image I_0, $\max_0 = \max(I_0(x(i, j)))$ and $\min_0 = \min(I_0(x(i,j)))$, and then calculate the noise level σ_0.

Step2: Judge whether double-discriminants $f_{cm} = (\max_0 - \min_0) < T_{mc}$ and $f_{c\sigma} = \sigma_0 < T_{\sigma c}$ are true or not. If they are true simultaneously, decomposition stops; otherwise decompose the initial image into four regions. Then use the new regions to replace I_0 one by one and return to step 1. Decomposition does not stop until two discriminants are true simultaneously for all regions.

Since the region consists of multiple classes, when using the classical QuadTree decomposition, the random mutations of pixel value caused by speckle may make discriminant $f_{cm} = (\max_0 - \min_0) < T_{mc}$ true; as a consequence, decomposition stops and details are lost. However, when using double-discriminants, the second discriminant $f_{c\sigma} = \sigma_0 < T_{\sigma c}$ is false for the region, which effectively enables the decomposition to continue.

The selection of T_{mc} and $T_{\sigma c}$ directly influences the final segmentation result. To get a better pixon-representation, our criterion of threshold selection is proposed as follows. For k classes segmentation, first do an initial segmentation, and then calculate the mean $m = \{m_1, \dots, m_k\}$ and the noise level $\sigma = \{\sigma_1 \dots \sigma_k\}$ of each class such that

$$T_{mc} = \min(m_i - m_j),\ 1 \leqslant i,\ j \leqslant k,\ i \neq j, \tag{5}$$

$$T_{\sigma c} = \min(\sigma_i),\ 1 \leqslant i \leqslant k. \tag{6}$$

T_{mc} defined by eq. (5) can avoid segmenting pixels belonging to different classes into the same class, and $T_{\sigma c}$ defined by eq. (6) can effectively suppress the influence of noise in stationary regions. The criterion above combines with the *a priori* knowledge of images, so it can choose different thresholds for different images automatically, suppressing the influence of noise.

We adopt the following simple experiment to verify the validity of the new QuadTree decomposition, as shown in Figure 2. Figure 2(a) is the observed image with speckle, Figure 2(b) is the result of classical QuadTree decomposition, and Figure 2(c) is the result of the new method. Experimental results indicate that for images with speckle noise, the classical QuadTree decomposition gets redundant pixons due to
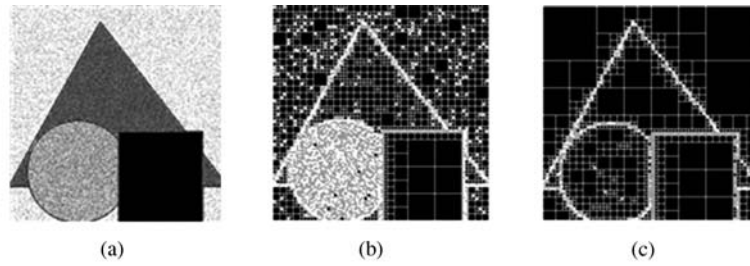
Figure 2 The QuadTree decomposition results of speckle noisy image. (a) Observed image with speckle (with variance noise 0.05); (b) the classical QuadTree decomposition method; (c) the new QuadTree decomposition method.

the influence of speckle, while our new method effectively suppresses the influence of speckle and obtains a satisfactory result because of the introduction of noise level.

3.2 Derivation of the new potential energy function of TMF based on pixon-representation of SAR images

A neighborhood system of pixon is defined by eq. (7). Let $\Omega = \{\omega_1, \ldots, \omega_k\}$ be the set of possible labels denoting the classes in the segment image and $L = \{l_1, \ldots, l_N\}$ be a family of random variables where $l_{i=1\cdots n} \in \Omega$ denotes the label of the ith pixon. The neighborhood cliques of pxion P_i are defined by eq. (8). $C(P_i)$ is the set of the neighborhood pixons P_j of P_i.

$$H(P_i) = \{\boldsymbol{n}_{i,j} | \boldsymbol{n}_{i,j} \in \boldsymbol{n}\}, \tag{7}$$

$$C(P_i) = \{P_j | P_j \in H(P_i)\}. \tag{8}$$

The expression of $W(x, u)$ in pixel level is given by eq. (4). Now we transform it into pixon level

$$W(x, u) = \sum_{(s,t) \in \mathbb{C}} \alpha(1 - 2\delta(x_s, x_t)) - (\beta\delta^*(u_s, u_t, a) + \gamma\delta^*(u_s, u_t, b))(1 - \delta(x_s, x_t)). \tag{9}$$

There are three parameters in eq. (9) in contrast with six in eq. (1). Because the size of each pixon is undetermined in the pixon-representation of images, there are no horizontal and vertical cliques, so we choose the same parameter for all cliques. Introducing the pixon intensity μ into potential energy function to weight δ function in eq. (9), we obtain potential energy of clique as follows:

$$V_c(\omega) = \frac{\theta_{i,j}}{\mu_i - \mu_j}, \tag{10}$$

$$\theta_{i,j} = \begin{cases} 0, & \mu_i = \mu_j, \\ 1, & \mu_i \neq \mu_j, \end{cases} \qquad \mu_i = \sum_{j=1}^{n_i} \frac{I(x_{i,j})}{n_i}, \tag{11}$$

where n_i is the number of pixels included in P_i, and $I(x_{i,j})$ is intensity of $x_{i,j}$. When the pixon intensities of pixons P_i and P_j are similar, and they have different labels, the clique potential associated with the pixons will be large. This means that the pixons having similar pixon intensities have high probability to receive the same label.

Finally, substituting eq. (10) into eq. (9) for the δ function, we obtain the energy function $W(x, u)$ based on pixon-representation:

$$\begin{aligned} W_p(x, u) &= \sum_{p^x{}_{i,j} \in H_x(p^x_j)} \sum_{p^u{}_{i,j} \in H_u(p^u_j)} \alpha(1 - V_{c,x}) - (\beta V'_{a,u} + \gamma V'_{b,u})(1 - V_{c,x}) \\ &= \sum_{p^x{}_{i,j} \in H_x(p^x_j)} \sum_{p^u{}_{i,j} \in H_u(p^u_j)} \alpha\left(1 - \frac{2 \times \theta_{i,j}}{\mu^x_i - \mu^x_j}\right) \\ &\quad - \left(\beta\frac{\theta^a_{i,j}}{\mu^u_i + \mu^u_j - 2a} + \gamma\frac{\theta^b_{i,j}}{\mu^u_i + \mu^u_j - 2b}\right)\left(1 - \frac{\theta_{i,j}}{\mu^x_i + \mu^x_j}\right). \end{aligned} \tag{12}$$

$\theta_{i,j}$, $\theta_{i,j}^a$ and $\theta_{i,j}^b$ are binary piecewise functions

$$\theta_{i,j} = \begin{cases} 0, & \mu_i = \mu_j, \\ 1, & \mu_i \neq \mu_j, \end{cases} \qquad \theta_{i,j}^a = \begin{cases} 1, & \mu_i^u = \mu_j^u = a, \\ 0, & \mu_i^u \neq \mu_j^u \neq a, \end{cases} \qquad \theta_{i,j}^b = \begin{cases} 1, & \mu_i^u = \mu_j^u = b, \\ 0, & \mu_i^u \neq \mu_j^u \neq b, \end{cases} \tag{13}$$

where μ_i^x and μ_i^u denote the intensity of the center pixon in field X and field U respectively, while μ_j^x and μ_j^u denote the intensity of the neighbor pixon in field X and field U respectively.

The forms of $W'(\varphi(x, y))$ and $\sum_{s \in S} \log |\frac{\partial(G^{-1} \circ H_{x_s}(y_s))}{\partial y_s}|$ are also transformed to meet the model based on pixon-representation. For each $P_i \in P$, put $Y_p = H_X^{-1} \circ G(Y_p')$. Then we obtain the distribution of (X, U, Y) as follows:

$$p(x, u, y) = \gamma \exp \left[- W_p(x, u) - W'(\varphi(x, y)) + \sum_{P_{i,j} \in H(p)} \log \left| \frac{\partial(G^{-1} \circ H_{x_{p_i}}(y_{p_i}))}{\partial y_{p_i}} \right| \right]. \tag{14}$$

3.3 Parameter estimation for fast TMF algorithm

In this paper, we use iterative conditional estimation (ICE) [8, 18] to estimate the parameters of the overall algorithm. As X is not observable, we have to use $Y = y$. The method runs as follows.

1. Initialize the searched parameters and the densities associated with the classes by some simple method.

2. At each iteration q, obtain the next parameters and densities associated with the classes from $Y = y$ and current parameters and densities in the following way.

a) simulate (x^{q+1}, u^{q+1}) according to $p(x, u|y)$ based on the current parameters;

b) use (x^{q+1}, u^{q+1}) to estimate α to get the next α^{q+1};

c) for each $i = 1, \ldots, k$, set $P_i^{q+1} = \{P_i \in P | x_i^{q+1} = \omega_i$ and $(y_p^{q+1})_{P \in P^{q+1}}$ to calculate the $p(y_p|x_p = \omega_i)$;

d) use the densities $h_i^{q+1}(y_p) = p(y_p|x_p = \omega_i)$ to calculate the cumulative functions H_i^{q+1} and $Y_p^{q+1} = G^{-1} \circ H_{x_p^{q+1}}^{q+1}(Y_p)$ and use $y^{q+1} = (y_p^{q+1})_{p \in P}$ to estimate $\beta^{1,q+1}$.

3. Stop the procedure when the estimates become steady. Calculate the conditional expectation of the parameter on (X, Y). If the conditional expectation keeps nearly invariant, the estimates are considered as steady. The parameter estimation process is given in Figure 3(a) and the whole process of the fast TMF algorithm is given in Figure 3(b).

4 Experimental results and analysis

In this paper we choose two simulated images and four real SAR images to test the validity and popularity of the fast TMF algorithm. Test 1(a) is a simulated image 256×256 in size; it is corrupted by multiplicative speckle noise with variance 0.05, while Test 2(a) is 512×512 in size and with variance 0.5. The *a priori* knowledge of four real SAR images is shown in Table 1. The classes are hand-selected according to the *a priori* knowledge. The computer configuration in the experiments is Intel(R) Core(TM)2 Duo CPU with the frequency of 2.33 GHz. All the segmented images presented above are obtained using 150 MPM samples, each performed through 30 Gibbs sampler iterations.

The analysis and discussion of the segmentation of simulated image and real SAR images (see Figures 4 and 5) are as follows.

Figure 4 Test 1(c)–Test 2(c) and Figure 5 Case 1(b)–case 4(b) show the estimated $U = u$ by the fast TMF algorithm. The different values of U describe different possible stationarities of (X, Y). In our experiments, we consider two different stationarities and the estimated $U = u$ seems to indicate two kinds of areas really corresponding to two visually different stationarities.
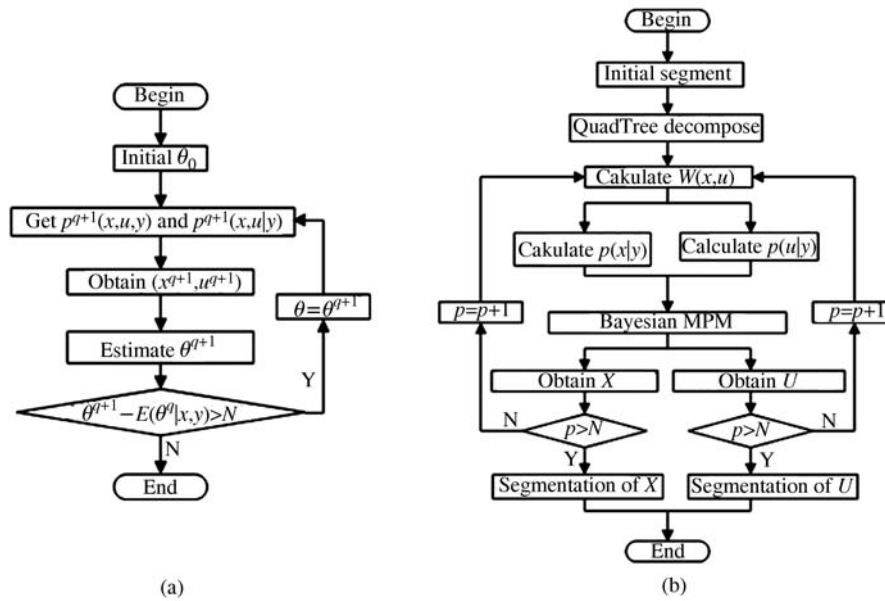
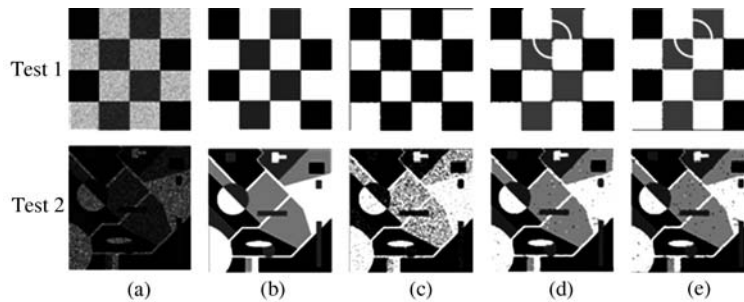**Figure 3**　(a) The process of parameter estimation; (b) the whole process of the fast TMF algorithm.

Figure 4　The segmentation results of the simulated SAR images. (a) Initial images with speckle noise; (b) manual segmentation; (c) estimated $U = u$; (d) non-Gaussian TMF segmentation; (e) the fast TMF algorithm.

Table 1　The *a priori* knowledge of the real SAR images

Image	Size	Band	Polarization	ENL	Classes	Image resource
Case 1	512×512	X	HH	2.9908	4	imaging data from a domestic airborne radar
Case 2	256×256	X	HH	3.9185	4	Jet Propulsion Laboratory
Case 3	256×256	X	HH	4.4523	4	DLR and EADS Astrium Company
Case 4	256×256	X	HH	7.2786	4	imaging data from a domestic airborne radar

4.1　Subjective and objective evaluation of two segmentation algorithms

In the segmentation results we mark the obviously different regions and edges between TMF and the fast TMF algorithm with yellow windows. From the results, we can see that: as shown in Figure 4, the edge location in Test 1(e) is more accurate than that in Test 1(d); in Test 2(d) and Test 2(e), the same segmentation performance is presented; as shown in Figure 5, Case 1(d) and Case 4(d) have smoother stationary regions and more accurate edges than Case 1(c) and Case 4(c); and there are more details in Case 2(d) than in Case 2(c). So we consider that the proposed fast algorithm performs as well as the TMF segmentation algorithm, or even better. Because of the use of the new QuadTree decomposition to decompose SAR images at different scales and reform an edge-based pixon-representation, this algorithm realizes a fast and efficient segmentation.
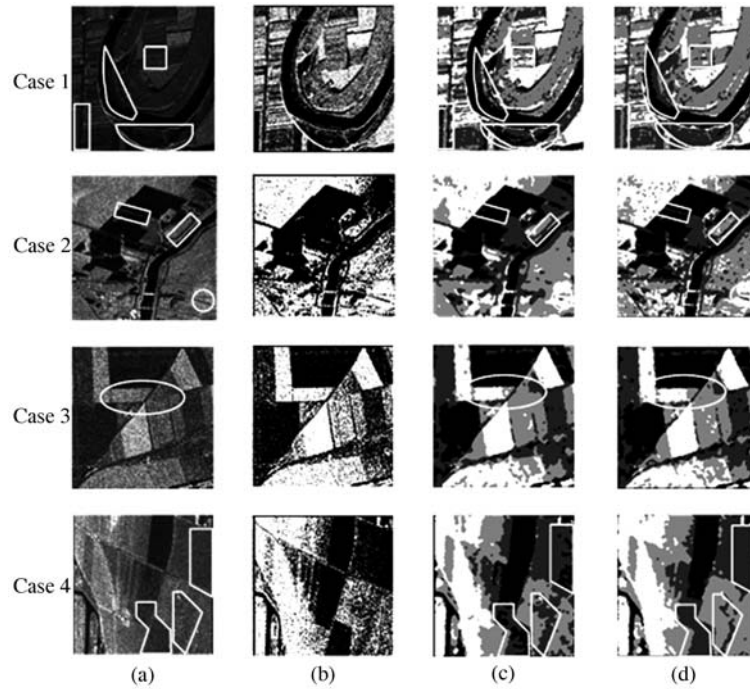
Figure 5 The segmentation results of real SAR images. (a) SAR images; (b) estimated $U = u$; (c) non-Gaussian TMF algorithm; (d) the fast TMF algorithm.

The objective evaluation criterion is given as follows: It contains three criterions of ration image, which are the logarithm of the normalized likelihood ratio D, the variance RI_{var} and the mean RI_{mean} [19]. D describes the region homogeneity of the segmentation results. The closer the value of D approaches 0, the better region homogeneity the segmentation results have. RI_{var} describes the change of the pixel value in the ratio image. The smaller the value, the better the performance of segmentation algorithm. RI_{mean} describes the situation of the suppression to speckle noise. The closer the value of RI_{mean} approaches 1, the better the suppression to speckle noise will be.

We analyze and discuss the segmentation of simulated data and real SAR images with three criterions of ration image above. As shown in Table 2, the fast TMF algorithm outperforms the non-Gaussian TMF segmentation method: the values of $|D|$ and RI_{mean} decrease obviously, which indicates that the regional homogeneity after segmentation is better, thus making the region smoother; the value of RI_{mean} is closer to 1, which shows that the fast TMF segmentation algorithm can suppress the speckle noise more effectively. The subjective evaluation consists with the objective evaluation , which fully indicates the effectiveness and the universality of the fast TMF algorithm.

4.2 Comparison of computational complexity between the two algorithms

In this paper, a new QuadTree decomposition method is proposed to realize multiscale decomposition to SAR images, which has smooth regions at coarse scale, and edges at fine scale. In this way, the amount of data to be processed is effectively reduced, while edges and details are maintained. Table 3 lists the number of pixels, the number of pixons and the ratios of the numbers of pixons to pixels. From Table 3, we can see that the number of pixons is only 5.32%–44.09% of that of pixels. That means that the amount of data to be processed is greatly reduced. We can also find that the reduction in the amount of data depends mainly on the complexity of image information. When there are more edges and details, or strong speckle noise in the image, then more pixons are required, and vice versa.

4.3 Comparison of computational cost between the two algorithms

Table 4 shows a comparison of required computational time between TMF algorithm and our fast TMF algorithm. From Table 4, we can conclude that the computational cost decreases substantially when new

Table 2   Comparision of segmentation performance between the two algorithms

Image	Non-Gaussian TMF algorithm			The fast TMF algorithm		
	$\|D\|$	RI_{mean}	RI_{var}	$\|D\|$	RI_{mean}	RI_{var}
Test 1	0.4140	1.0032	0.3687	0.3210	1.0267	0.2745
Test 2	0.7826	1.0355	0.3662	0.7705	1.0533	0.1372
Case 1	1.1079	1.0182	0.2691	0.9278	1.0477	0.2678
Case 2	0.3902	1.0292	0.1632	0.1521	1.0308	0.0677
Case 3	0.2497	1.0294	0.0887	0.2114	1.0327	0.0730
Case 4	0.1815	1.0077	0.0541	0.1810	1.0107	0.0463

Table 3   Ratios between the numbers of pixels and pixons

Image	The number of pixels	The number of pixons	Ratios between the numbers of pixons and pixels(%)
Test 1	65536	3484	5.32
Test 2	262144	115588	44.09
Case 1	262144	44551	16.99
Case 2	65536	19255	29.38
Case 3	65536	9073	13.84
Case 4	65536	11743	17.92

Table 4   Comparison of computational cost between the two algorithms

Image	Size of image	Cost of TMF algorithm(s)	Cost of the fast TMF algorithm(s)
Test 1	256×256	49.177021	28.398844
Test 2	512×512	305.223631	216.629987
Case 1	512×512	245.789907	207.385674
Case 2	256×256	61.423555	43.098125
Case 3	256×256	61.369764	36.014619
Case 4	256×256	61.714754	34.011161

pixon-representation of SAR image is incorporated into the image segmentation process. So our algorithm is an effective fast algorithm.

5   Conclusions

In this paper, we have proposed a fast algorithm based on TMF for unsupervised multi-class segmentation of SAR images. For the speckle noise in SAR images, we introduce the region noise level into the classical QuadTree decomposition, and then establish several new criterions for decomposition discriminant and threshold selection. With the new QuadTree decomposition, a SAR image can quickly be mapped into an edge-based pixon-representation. Then by combining TMF model with the pixon-representation of SAR image, a new potential energy function of TMF based on pixon-representation is derived. Finally, the segmentation is finished by Bayesian MPM. Our fast TMF algorithm is applied to segment simulated data and real SAR images. Experimental results and analysis demonstrate that the fast TMF algorithm can be comparable with, or even outperform the TMF segmentation algorithm, but with significantly reduced computational cost and greatly improved efficiency. Especially when dealing with SAR images in large size, the fast TMF algorithm can give a real-time, and robust and efficient result of segmentation.

References

1 Giordana N, Pieczynski W. Estimation of generalized multisensor hidden Markov chains and unsupervised image segmentation. IEEE Trans Pattern Anal Mach Intell, 1997, 19: 465–475

2 Poggi G, Scarpa G, Zerubia J. Supervised segmentation of remote sensing images based on a tree-structured MRF model. IEEE Trans Geosci Remote Sens, 2005, 43: 1901–1911

3 Benboudjema D, Tupin F, Pieczynski W, et al. Unsupervised segmentation of SAR images using triplet Markov fields and Fisher noise distributions. In: IEEE International Geoscience and Remote Sensing Symposium, Barcelona, Spain, 2007. 3891–3893

4 Benboudjema D, Pieczynski W. Multisensor triplet Markov fields and theory of evidence. Image Vision Comput, 2006, 24: 61–69

5 Lanchantin P, Pieczynski W. Unsupervised segmentation of triplet Markov chains hidden with long-memory noise. Adv Concepts Intell Vision Syst, 2008, 88: 1134–1151

6 Blanchet J, Forbes F. Triplet Markov fields for the classification of complex structure data. IEEE Trans Pattern Anal Mach Intell, 2008, 30: 1055–1067

7 Benboudjema D, Pieczynski W. Unsupervised image segmentation using triplet Markov fields. Comput Vision Image Understand, 2005, 99: 476–498

8 Benboudjema D, Pieczynski W. Unsupervised statistical segmentation of nonstationary images using triplet Markov fields. IEEE Trans Pattern Anal Mach intell, 2007, 29: 1367–1378

9 Benboudjema D, Pieczynski W. Segmenting non stationary images with triplet Markov fields. In: International Conference on Image Processing (ICIP2005), Geneva, Italy, 2005. 11–14

10 Benboudjema D, Pieczynski W. Unsupervised segmentation of non stationary images with non Gaussian correlated noise using triplet Markov fields and the Pearson system. In: Proc. IEEE Int'l Conf. Acoustics, Speech, and Signal Processing, Vol. 2, Toulouse, France, 2006

11 Pieczynski W. Multisensor triplet Markov chains and theory of evidence. Int J Approx Reason, 2007, 45: 1–16

12 Pina R K, Puetter R C. Bayesian image reconstruction: the pixon and optimal image modeling. PASP, 1993, 105: 630–637

13 Yang F, Jiang T. Pixon-based image segmentation with Markov random fields. IEEE Trans Image Process, 2003, 12: 1552–1559

14 Lin L, Zhu L, Yang F, et al. A novel pixon-representation for image segmentation based on Markov random field. Image Vision Comput, 2008, 26: 1507–1514

15 Papila I, Yazgan B. An unsupervised segmentation method based on MPM for SAR images. Geosci Remote Sens Lett, 2005, 2: 55–58

16 Jedynak B, Zheng H, Daoudi M. Skin detection using pairwise models. Image Vision Comput, 2005, 23: 1122–1130

17 Geman S, Geman D. Stochastic relaxation, Gibbs distributions and the Bayesian restoration of images. IEEE Trans Pattern Anal Mach Intell, 1984, 6: 721–741

18 Ibanez M V, Simo A. Parameter estimation in Markov random field image modeling with imperfect observations: A comparative study. Pattern Recognit Lett, 2003, 24: 2377–2389

19 Caves R, Quegna S, White R. Quantitative comparison of the perfomance of SAR segmentation algorithms. IEEE Trans Image Process, 1998, 7: 1534–1546